PERGAMON

International Journal of Heat and Mass Transfer 45 (2002) 5035–5044

International Journal of HEAT and MASS TRANSFER

www.elsevier.com/locate/ijhmt

Performance of the herringbone wavy fin under dehumidifying conditions

Yur-Tsai Lin [a], Young-Ming Hwang [a], Chi-Chuan Wang [b,*]

[a] Department of Mechanical Engineering, Yuan-Ze University, Taoyuan, Taiwan

[b] D400 ERL/ITRI Energy and Resources Laboratories, Industrial Technology Research Institute, Building 64, 195-6 Section 4, Chung Hsing Road, Hsinchu, Taiwan 310, ROC

Received 17 December 2001; received in revised form 7 May 2002

Abstract

An experimental study reporting the airside performance of the herringbone wavy fin geometry in wet conditions is conducted. In the visualization of the condensate flow pattern, a very special "locally dry" spot of the corrugation wavy channel having a corrugation angle of 15° and a fin spacing of 8.4 mm is seen. This phenomenon is related to the recirculation of the airflow across the apex. Conversely, this phenomenon is not so clearly seen either for a fin pitch of 2.6 mm with a corrugation angle of 15° or a corrugation angle of 25°. Flow visualization of the non-uniform distribution of the condensation in the facets results in a dependence between axial length and friction factor. Based on the present test results, airside performance in terms of Nusselt number and Fanning friction factor for the present herringbone wavy fin geometry in wet conditions are developed. The mean deviations of the proposed correlations are 2.52% and 4.81%, respectively.

Keywords: Augmentation; Dehumidifying heat exchanger; Finned surfaces

1. Introduction

Corrugated or wavy wall surfaces are often employed as a passage in the heat exchanger device for the purpose of heat transfer enhancement. In practical implementation of the corrugated channels, two variants are often employed, namely the herringbone wavy and smooth wavy. As seen in Fig. 1, the major difference between the herringbone and smooth wavy fin is the sharp edge corner. In this study, efforts are focused on the herringbone wavy fin geometry. Investigations of the herringbone wall channels had been conducted both numerically and experimentally during the past several decades [1–10].

For numerical investigations, Amano [1] developed a modified hybrid scheme that is capable of handling both laminar and turbulent flow regime. His results indicated a negligible influence of the step ratio on the local Nusselt number if the step ratio is above 3. Ramadhyani [2] and Asako and Faghri [3] also adopted a steady-state formulation of the wavy channel, Ramadyani's calculations indicated that for a smaller corrugation angle like $\theta = 15°$ there is no appreciable heat transfer augmentation, and he further suggested that to obtain an appreciable heat transfer enhancement, the corrugation angle should be at least 20°. Based on a finite volume methodology, Asako and Faghri [3] performed a non-orthogonal transformation to investigate the performance of a corrugated wavy channel in fully developed flow regime. Their numerical results revealed smaller difference in the heat transfer rate ratios between constraints of fixed pumping power, fixed pressure drop, and fixed mass flow rate. Yang et al. [4] later extends the numerical methods of [3] to the transitional region ($2500 > Re > 100$) for $\theta = 15°$ and 30° with three interwall spacings. They also conducted a flow visualization to verify their numerical results. They reported that

* Corresponding author. Tel.: +886-3-5916-294; fax: +886-3-5820-250.

E-mail address: ccwang@itri.org.tw (C.-C. Wang).

0017-9310/02/$ - see front matter
PII: S0017-9310(02)00193-X

Nomenclature

A_c	minimum free-flow area (m^2)
A_f	fin surface area (m^2)
A_0	total surface area (m^2)
$n1$, $n2$, $n3$, $n4$	correlation parameters, dimensionless
D_h	hydraulic diameter, $4A_cL/A_0$ (m)
f	friction factor, dimensionless
$f1$, $f2$, $f3$, $f4$	correlation parameters, dimensionless
F_s	fin spacing (m)
G_c	mass flux of the air based on the minimum flow area ($kg/m^2\,s$)
h_0	sensible heat transfer coefficient ($W/m^2\,K$)
k	thermal conductivity (W/m K)
K_c	abrupt contraction pressure-loss coefficient
K_e	abrupt expansion pressure-loss coefficient
L	depth of the corrugation channel (m)
$\dot{m}_a$	air mass flow rate (kg/s)
N	number of longitudinal tube rows, dimensionless
Nu	Nusselt number based on hydraulic diameter
P_d	wave height (m)
$\dot{Q}_a$	sensible heat transfer rate (W)
RH_{in}	inlet relative humidity
Re	Reynolds number based on hydraulic diameter, dimensionless
Re_{crit}	critical Reynolds number for condensate carry-over
T_a	air temperature (°C)
$\overline{T}_b$	average base temperature (°C)
$\overline{T}_{fin}$	average fin temperature (°C)
ΔT_{LM}	log mean temperature difference (°C)
V_{fr}	frontal velocity (m/s)
X_f	projected fin length (m)
η_f	fin efficiency, dimensionless
η_0	surface efficiency, dimensionless
θ	corrugation angle (°)
θ_A	advancing contact angle (°)
θ_R	receding contact angle (°)
δ_f	fin thickness (m)
ρ	mass density of fluid (kg/m^3)
σ	contraction ratio of cross-sectional area

Subscripts

dry	dry condition or dry bulb temperature
fb	fin base
in	inlet
m	mean value
out	outlet
wet	wet condition or wet bulb temperature

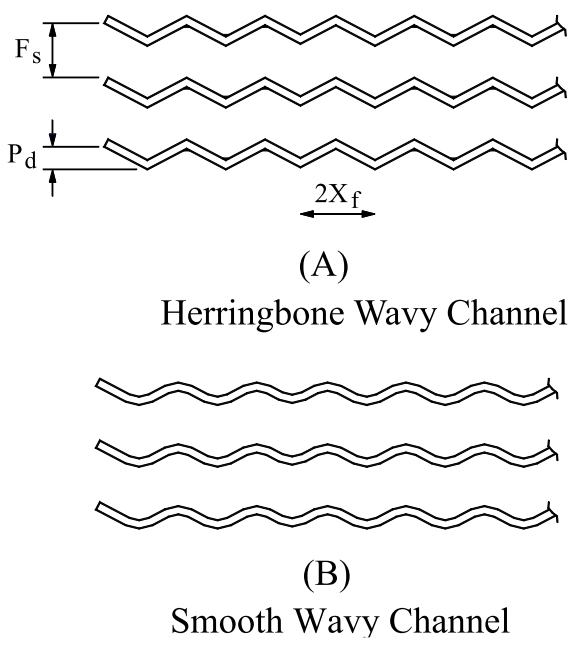

Fig. 1. Schematic of the herringbone wavy channel and smooth wavy fin channel.

the location of the transition to turbulent flow is a function of axial cycles and an asymptote of the transition point of $Re = 200$. The above studies were associated with performance in the corrugated wavy channel alone. In practice, wavy channels are often accompanied with tubes. In this regard, the numerical studies by Jang and Chen [5], McNab et al. [6], and Min and Webb [7] were performed to investigate the relevant parametric interactions in conjunction with tube and corrugated channel by commercially available CFD code. Basically, these investigations showed fair agreements with the experimental data.

Extensively experimental studies in connection with the wavy channel were also available in the literature [8–11]. The pioneer work by Goldstein and Sparrow [8,9] provided detailed data of the herringbone wavy channel. They used a mass transfer analogy to investigate the heat transfer characteristics of corrugated channel by exploitation the sublimation of naphthalene. Their test ranges covered the laminar, transition, and turbulent flow regime. They reported that the corrugated channel can improve the heat transfer, but accompanied with an even higher pressure drop penalty. Their flow visualization found the presence of longitudinal vortex, and concluded that the herringbone wavy channel is effective

only in turbulent flow region. Ali and Ramadyani [11] performed a flow visualization by dye injection in two herringbone fin geometries. They noticed a wavering of the dye-line, suggesting that the flow is unsteady.

The aforementioned studies were performed in the absence of condensation. For heat exchangers operated as the evaporators or cooling coils of air-conditioning equipment, the surface temperature of the fins may be below the dew point temperature. In this regard, the presence of water condensate will certainly complex the flow phenomenon. Unfortunately, the only experimental work in connection with the herringbone wavy fin under dehumidifying conditions were by Mirth and Ramadhyani [12] and Wang et al. [13,14], who presented test results and correlations from commercially available fin-and-tube heat exchangers. These investigations provided some useful performance data but lacked of detailed physical insight. In view of this concern, it is main objective of this study is to explore this basic condensation phenomenon in the herringbone wavy channel via experimental approach.

2. Experimental apparatus

Experiments were performed in an environmental chamber as shown in Fig. 2. The test apparatus is based on the air–enthalpy method proposed by ANSI/ASHRAE Standard 37 [15]. Cooling capacity was measured from the enthalpy difference of the air flow rate across the test sample. The airflow measuring apparatus is constructed from ASHRAE Standard 41.2 [16]. Dry and wet bulb temperature measurement devices of the airflow is constructed based on ASHRAE Standard 41.1 [17]. Schematic diagram of the experimental air circuit assembly is also shown in Fig. 2. Experiments were performed in an environmental chamber. The environmental chamber can control the ambient conditions in the range of $10 \leqslant T_{dry} \leqslant 50°C$ and $40\% \leqslant RH_{in} \leqslant 95\%$. Control resolution for the related dry bulb and wet bulb temperature is 0.1 °C.

To perform the visual observations of the condensate, models of corrugated surface was designed and fabricated as shown in Fig. 3. A total of four test samples were manufactured for testing. Their detailed geometry is tabulated in Table 1. The aluminum alloy 6061 is chosen as the base and fin material because of its relatively high thermal conductivity and rigidity. Contact angle of the test surfaces were measured by the CHAN dynamic contact angle analyzer using the Wilhelmy plate technique. The measured contact angles of the test samples in terms of advancing and receding contact angles (θ_A and θ_R) are tabulated in Table 1. Uncertainty of the contact angle measurement is less

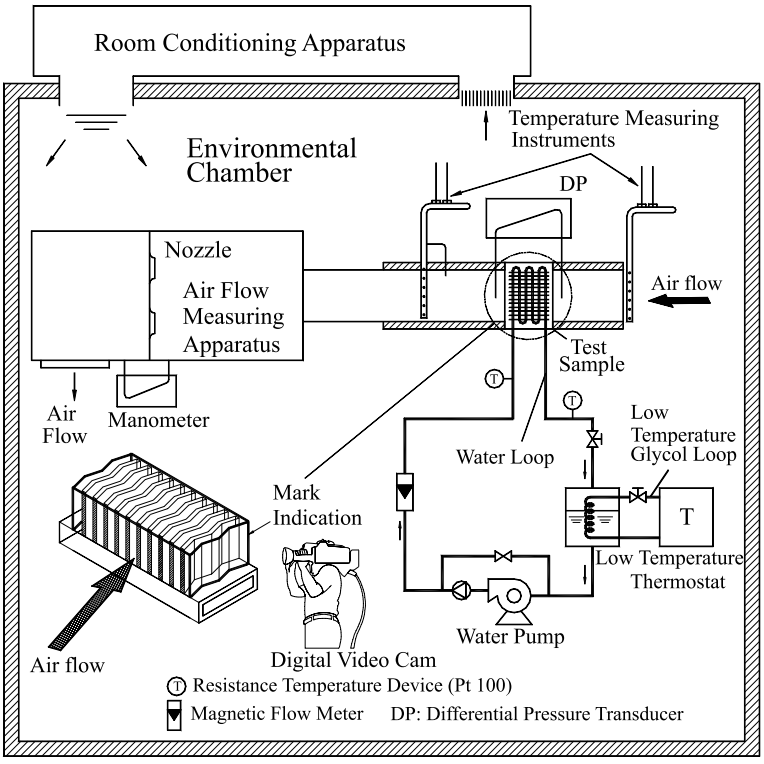

Fig. 2. Schematic of experimental setup.

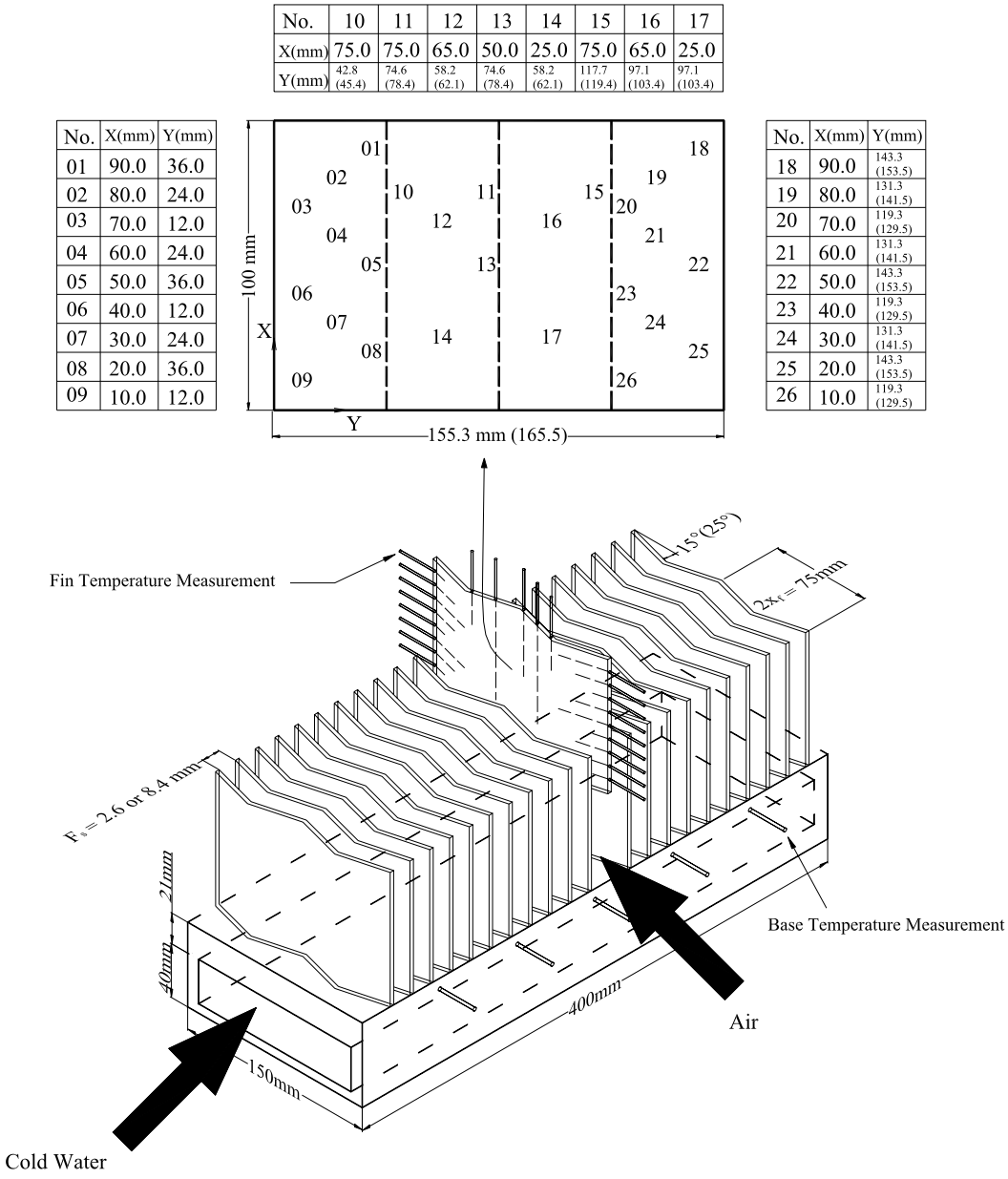

Fig. 3. Enlarged view of the test section.

Table 1
Geometric specification of the test samples

Variant	θ (°)	F_s (mm)	δ_f (mm)	P_d (mm)	X_f (mm)	D_h (mm)	σ	θ_A (°)	θ_R (°)
1	25	2.6	3.2	17.5	37.5	5.5	0.496	92.4	48.0
2	25	8.4	3.2	17.5	37.5	16.6	0.752	92.8	51.4
3	15	2.6	3.2	10.0	37.5	5.7	0.488	92.7	54.2
4	15	8.4	3.2	10.0	37.5	16.9	0.744	92.6	50.1

than 2°. The fin is 150 mm deep, 100 mm wide, and 3.2 mm thick. As shown in Fig. 3, the fins were mounted vertically on the aluminum alloy block. The herringbone channel along the base was machined to seat the cor-

Table 2
Summary of estimated uncertainties

Primary measurements		Derived quantities		
Parameter	Uncertainty	Parameter	Uncertainty $V_{fr} = 0.3$ m/s	Uncertainty $V_{fr} = 6$ m/s
$\dot{m}_a$	0.3–1%	Re_{D_h}	±1.0%	±0.5%
T_a	0.1 °C	$\dot{Q}_a$	±5.2%	±2.1%
RH_{in}	2%	η_f	±4.5%	±3.3%

rugate fins. The base block was carefully machined to have 63 herringbone channels. The width and height of the groove is 3.2 mm. Noticed that a high thermal conductivity grease ($k = 2.1$ W/m K) was used to connect the fin and the base material to minimize the contact resistance. A mean gap distance of 0.05 mm is assumed between the attached fin and the base aluminum block. Actual fin base temperatures were then corrected from the measured temperatures. The fin spacing can be either 2.6 or 8.4 mm. To measure the fin temperature in both directions of the transverse and longitudinal to the airflow, a total of 26 thermocouples were inserted in one of the fins. Detailed locations of the thermocouples were shown in Fig. 3. These 'T'-type thermocouples were pre-calibrated with a resolution of 0.1 °C. To heat and cool the fin, water was circulated through the rectangular duct drilled beneath the fin base in the aluminum block. The water inlet temperature of the test section was controlled by low temperature thermostat. During the experiments, water was circulated with a sufficiently high velocity (>3 m/s) to maintain the fin base temperature at a constant level. For various operation frontal velocities, the thermostat temperature was adjusted to keep the variation of the fin base temperature between inlet and outlet to be less than 0.3 °C. The test conditions are given as follows:

Inlet dry bulb temperature: 20–27 °C.
Inlet relative humidity: 40–90%.
Water temperature at the inlet: 2–9 °C.
Fin base temperature: 7–13 °C.

Droplet formulation on the fin was recorded by a JVC digital video cam DVM50u with a speed of 30 frames/s. Experimental uncertainties are tabulated in Table 2.

3. Data reduction

The average frontal velocity, V_{fr}, was calculated by dividing the measured volumetric flow rate by the inlet cross-section area. The Reynolds number is based on the hydraulic diameter D_h $(= 4A_cL/A_0)$. The sensible heat transfer rate is calculated from the inlet and outlet temperatures across the test section, namely,

$$\dot{Q}_a = \dot{m}_a c_{p,a}(T_{a,in} - T_{a,out}) \tag{1}$$

Determination of the sensible heat transfer coefficient, h_0, is as follows:

$$\dot{Q}_a = h_0 \eta_0 A_0 \Delta T_{LM} \tag{2}$$

where ΔT_{LM} is the log mean temperature difference,

$$\Delta T_{LM} = \frac{((T_{a,out} - T_{fb,in}) - (T_{a,in} - T_{fb,out}))}{\ell n\left(\frac{T_{a,out} - T_{fb,in}}{T_{a,in} - T_{fb,out}}\right)} \tag{3}$$

The η_0 in Eq. (2) is the surface efficiency, and is related to the fin surface area, total surface area, and fin efficiency:

$$\eta_0 = 1 - \frac{A_f}{A_0}(1 - \eta_f) \tag{4}$$

where η_f is the fin efficiency which is obtained as follows:

$$\eta_f = \frac{T_a - \overline{T}_{fin}}{T_a - \overline{T}_b} \tag{5}$$

The airside performance of the herringbone wavy channel can be in terms of non-dimensional quantities of Nusselt number and Fanning friction factor:

$$Nu = \frac{h_0 D_h}{k} \tag{6}$$

$$f = \frac{A_c}{A_0}\frac{\rho_m}{\rho_{in}}\left[\frac{2\rho_{in}\Delta P_0}{G_c^2} - \left(K_c + 1 - \sigma^2\right) - 2\left(\frac{\rho_{in}}{\rho_{out}} - 1\right) + \left(1 - \sigma^2 - K_e\right)\frac{\rho_{in}}{\rho_{out}}\right] \tag{7}$$

4. Results and discussion

In the visualization study, photographs were taken for frontal velocities ranging from 0.3 to 6 m/s. The corresponding dry bulb temperature at the inlet were maintained at 27 °C, while the inlet wet bulb temperature is maintained at 19, 22, and 25 °C, respectively. Selected photographs from the observations for $F_s = 2.6$ mm at $T_{wet} = 25$ °C are shown in Fig. 4 with the corrugation angle of 15° and 25°.

In Fig. 4, at a high frontal velocities like 6 or 4 m/s, one can clearly see the inclination line indicating the

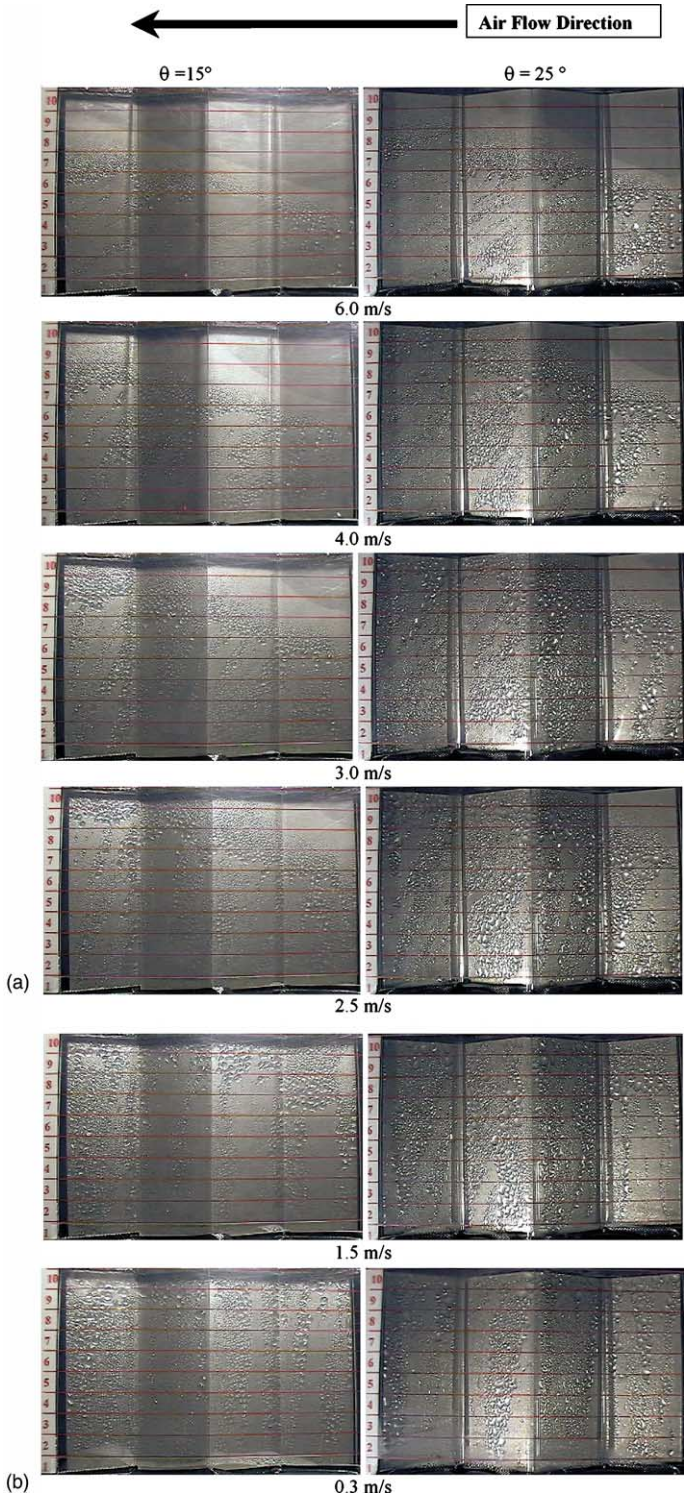

Fig. 4. Droplet formation on a wavy fin for corrugation angle of 15° and 25° ($T_{dry} = 27$ °C, $T_{wet} = 25$ °C).

dry–wet boundary located at the vicinity of the entrance region. Apparently, for the partially wet condition, the dry–wet boundary line for the corrugation angle of 15° is notably lower than that of 25°. The results imply

better heat transfer characteristics of the larger corrugation angle. Note that the drop size near the boundary is very fine and the drop size increases as the distance is approached to the fin base. The very fine size of droplet may grow up in the down stream of airflow and join with the neighboring droplet to become larger droplets. As a consequence, the larger droplet grew more quickly to a critical size, overcoming the force due to surface tension, eventually falls off to the fin base. However, due to the presence of larger vapor shear at $V_{fr} = 4.0$ and 6.0 m/s, the path of condensate drainage is inclined to the flow direction. In this regard, some of the condensate is shown to be blown out the corrugated channel subjected to strong vapor shear. Conversely, this inclined condensate drainage phenomenon is less profound for a wider fin spacing of 8.4 mm. Usually, the condensate drains vertically from the upper portion of the fin to the bottom for a fin spacing of 8.4 mm and $V_{fr} < 4$ m/s. This phenomenon becomes more pronounced with larger corrugation angle and smaller fin spacing. A visual examination of the observed critical Reynolds number that causing the "blow-off" of the condensate is correlated by the following equation.

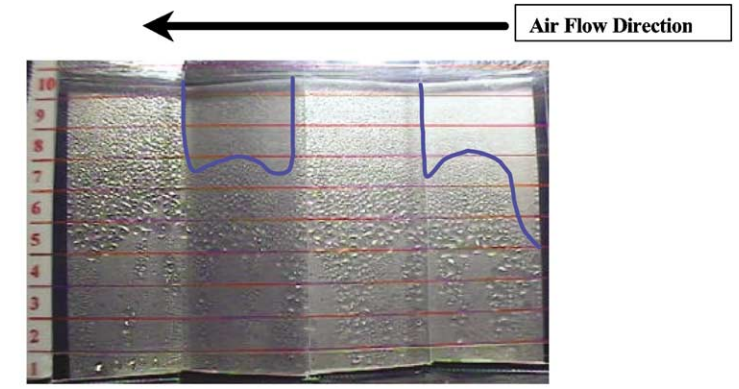

(a) $\theta = 15°$, $T_{dry} = 27$ °C, $T_{wet} = 22$ °C, $F_s = 8.4$ mm, $V_{fr} = 1.0$ m/s.

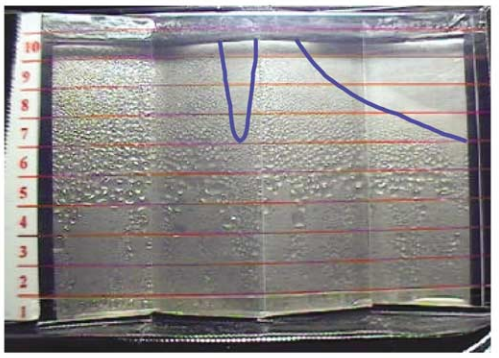

(b) $\theta = 15°$, $T_{dry} = 27$ °C, $T_{wet} = 22$ °C, $F_s = 8.4$ mm, $V_{fr} = 3.0$ m/s.

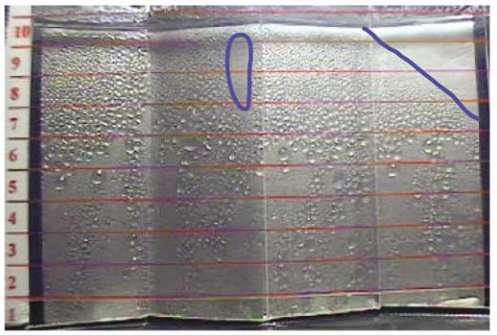

(c) $\theta = 15°$, $T_{dry} = 27$ °C, $T_{wet} = 25$ °C, $F_s = 8.4$ mm, $V_{fr} = 6.0$ m/s.

Fig. 5. Photos of locally dry spot phenomena.

$$Re_{\mathrm{crit}} = 688.58\theta^{0.7892}\mathrm{RH}^{-1.4023}\left(\frac{P_{\mathrm{d}}}{F_{\mathrm{s}}}\right)^{-1.2346} \quad (8)$$

To describe the details of the phenomena of condensate flow, definition of the corrugated channel as consisting of convex and concave corrugations must be given. The tip of the convex corrugation is called "apex" and the root of a concave corrugation is the "antapex". In this study, a very special "locally dry" spot of the corrugation wavy channel for the corrugation angle of 15° and a fin spacing of 8.4 mm is seen. As shown in Fig. 5, the locally dry spot is observed just behind the apex of the corrugation. In this nearly dry spot, droplet is too fine to identify and there is no condensate drainage phenomenon in this region. Notice that this special phenomenon is not so clearly seen either for a fin spacing of 2.6 mm with a corrugation angle of 15° or a corrugation angle of 25°. This phenomenon can be explained from the numerical visualization performed by McNab et al. [6]. As shown in Fig. 6 from their numerical visualization which reported large regions airflow separation of recirculating flow across the apex when the bulk of the airflow passes across the center of the channel. If the corrugation angle is increased, as shown in Fig. 6b, one can see the flow changes direction after impingement of the second facet and the velocity component parallel to the wall increases, creating a region of flow acceleration nearby the apex. Thus, the flow-recirculation phenomenon is less pronounced. In this regard, one can expect this locally dry spot is not so pronounced for the conditions of smaller fin spacing or larger corrugation angles. However, despite the flow circulation phenomenon is not so pronounced at a larger corrugation angles, the airflow impingement on the first and third facet of the corrugation apparently improved the bulk motion toward the wall surface. Therefore, the condensate drainage on the second and fourth facet is much more pronounced than that on the first and third facet.

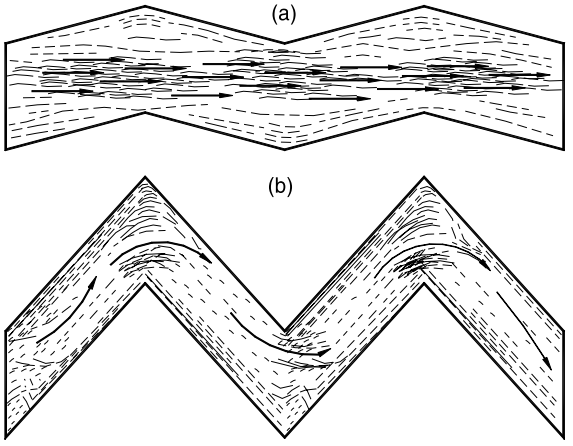

Fig. 6. Schematic of the numerical simulation of herringbone wavy channels by McNab et al. [6].

The above observation of the condensate flow pattern implies a non-uniform condensation phenomenon in the airflow direction. This is because the airflow in front of the apex receives much more condensate than the airflow after the apex. Since more condensate will result in larger friction in the impingement side whereas less condensate is in the leeside. The non-uniform condensate phenomenon eventually leads to a non-uniform skin friction distribution along the airflow direction, suggesting the friction factor of the wavy channel in wet conditions depends on the axial length. This unusual phenomenon is not seen for plain fin surfaces or highly interrupted surfaces such as louver and slit. In the open literature, test data of the herringbone fin surface reporting a dependence of the axial length or the number of tube row had been reported by the Mirth and Ramadhyani [12] and Wang et al. [13]. However, Mirth and Ramadhyani [12] did not provide any explanation while Wang et al. [13] suspects the condensate may alter the flow filed that leads to this consequence. Based on the present flow visualization, it is likely that this phenomenon is related to the non-uniform condensation caused by the wavy corrugation.

Fig. 7 shows the measured results of the heat transfer performance and the pressure drop vs. inlet air frontal velocity, V_{fr}, of the test samples. Results of Fig. 7a is for $\theta = 15°$ while Fig. 7b is for $\theta = 25°$. The corresponding dry and wet bulb temperatures are 27 and 25 °C, respectively. As shown in the figure, larger corrugation angle and smaller fin spacing will result in higher heat transfer coefficients and larger pressure drops. In general, the heat transfer coefficient in wet conditions relative to that in dry condition ($h_{0,\mathrm{wet}}/h_{0,\mathrm{dry}}$) increases slightly with the frontal velocity. However, this ratio reaches an asymptotic value of 1.5–1.7 near $V_{\mathrm{fr}} = 4$ m/s. The results is roughly the same for both $F_{\mathrm{s}} = 2.6$ and 8.4 mm. Converse to the test results of heat transfer coefficients, the ratios of $\Delta P_{\mathrm{wet}}/\Delta P_{\mathrm{dry}}$ for $F_{\mathrm{s}} = 2.6$ mm peak at a frontal velocity near 2.5 m/s. This phenomenon is also roughly the same for both $\theta = 15°$ and 25°. In contrast with the previous results, test results of $F_{\mathrm{s}} = 8.4$ mm did not reveal this phenomenon. The results can be explained from the visual results of Fig. 4. For a frontal velocities above 2.5 m/s, one can clearly see a "partially-dry" portion occurred near the upper region of the entrance. As reported by some investigators [12–14], the pressure drops in wet conditions are considerably higher than that in dry conditions due to the presence of water condensate. Accordingly, the increase of pressure drops relative to dry conditions increases with inlet wet bulb temperature and smaller fin spacing because of pronounced condensate loading. For a fin spacing of 2.6

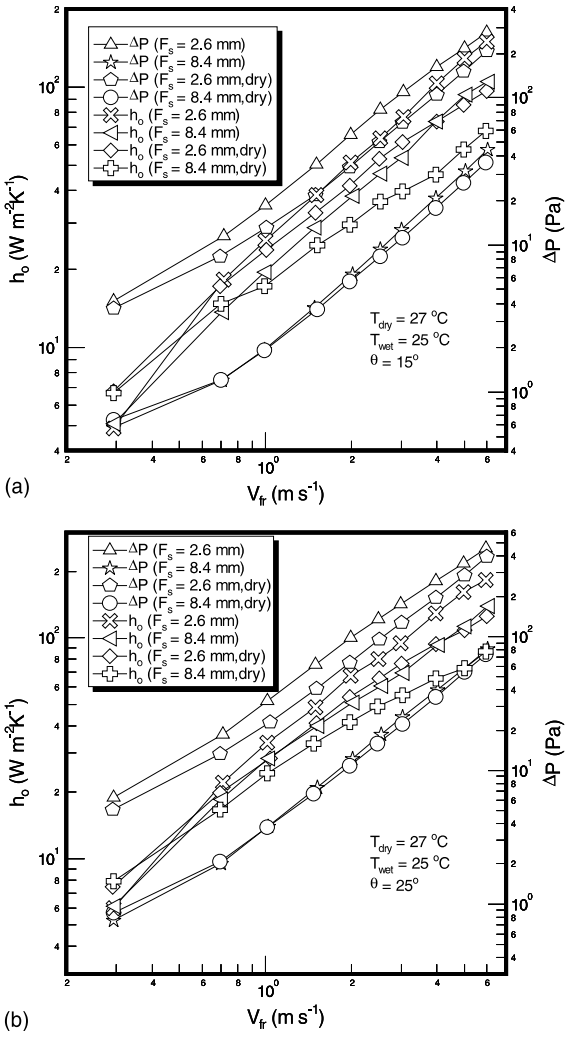

Fig. 7. Airside performance of the herringbone wavy fin in wet conditions; (a) $\theta = 15°$; (b) $\theta = 25°$.

mm and $V_{fr} \geqslant 2.0$ m/s, the occurrence of dry spot will reduce the corresponding pressure drop considerably. In this regard, one can experience that the ratios of $\Delta P_{wet}/\Delta P_{dry}$ start to fall dramatically. On the contrary, for a fin spacing of 8.4 mm, the ratios of $\Delta P_{wet}/\Delta P_{dry}$ did not reveal a maximum value in the present test range. This is because the influence of condensate on the pressure drop is comparatively small for a wider spacing. In conclusion, for a smaller fin spacing like 2.6 mm, the ratios of $\Delta P_{wet}/\Delta P_{dry}$ start to decline when partially-wet conditions occur.

In order to quantify the airside performance of the corrugated wavy fin geometry in wet condition, a regression technique was performed to correlate the airside performance, the airside characteristics in dehumidifying conditions are in terms of Nusselt number and friction factor, respectively. Correlations are given as follows:

$$Nu = 0.02656 Re_{D_h}^{n1} \left(\frac{F_s}{D_h}\right)^{n2} \theta^{n3} \mathrm{RH}^{n4} \tag{9}$$

$$f = 0.02403 Re_{D_h}^{f1} \left(\frac{F_s}{D_h}\right)^{f2} \theta^{f3} \mathrm{RH}^{f4} \tag{10}$$

where

$$n1 = 0.92333 \tag{11}$$

$$n2 = 2.5906 \tag{12}$$

$$n3 = 0.47028 \tag{13}$$

$$n4 = 0.07773 \tag{14}$$

$$f1 = -0.41543 \tag{15}$$

$$f2 = -0.096529 \tag{16}$$

$$f3 = 1.3385 \tag{17}$$

$$f4 = -0.13035 \tag{18}$$

The mean deviations of the proposed correlations of Eqs. (9) and (10) are 2.52% and 4.81%, respectively.

5. Conclusions

An experimental study concerning the airside performance and the visualization of the condensate flow pattern of the herringbone wavy fin channel in wet condition is conducted. Based on the test results and observation, the following conclusions are made.

(1) A very special locally dry spot of the corrugation wavy channel for the corrugation angle of 15° and a fin spacing of 8.4 mm is seen. The locally dry occurs just behind the apex. This phenomenon is related to the recirculation of the airflow across the apex. Conversely, the locally dry phenomenon is not so clearly seen either for a fin spacing of 2.6 mm with a corrugation angle of 15° or a corrugation angle of 25°.
(2) Visual observation of the dehumidification suggests that the non-uniform condensation in front of the apex and the leeside causes a non-uniform distribution of the condensate. In this regard, the friction characteristics are related to the axial length of corrugated channel.
(3) Larger corrugation angle and smaller fin spacing will result in higher heat transfer coefficients and larger pressure drops. In the present test range, for a smaller fin spacing like 2.6 mm, the ratios of $\Delta P_{wet}/\Delta P_{dry}$ start to decline when the partially-wet conditions of the channel is encountered. This phenomenon is not

so clearly seen for a larger fin spacing of 8.4 mm due to the comparatively small influence of condensate.

(4) Airside performance in terms of Nusselt number and Fanning friction factor for the present herringbone wavy fin geometry in wet conditions are developed, the mean deviations of the proposed correlations are 2.52% and 4.81%, respectively.

Acknowledgements

The authors are indebted to the Energy R&D foundation funding from the Energy Commission of the Ministry of Economic Affairs and National Science Council (NSC 89-2212-E-155-014) of Taiwan for supporting this study.

References

[1] R.S. Amano, A numerical study of laminar and turbulent heat transfer in periodically corrugated channel, ASME J. Heat Transfer 107 (1985) 564–569.

[2] S. Ramadhyani, Numerical prediction of flow and heat transfer in corrugated ducts, ASME paper, HTD vol. 66, 1986, pp. 37–43.

[3] Y. Asako, M. Faghri, Finite-volume solutions for laminar flow and heat transfer in a corrugated duct, ASME J. Heat Transfer 109 (1987) 627–634.

[4] L.C. Yang, Y. Asako, M. Yamaguchi, M. Faghri, Numerical prediction of transitional characteristics of flow and heat transfer in a corrugated duct, ASME J. Heat Transfer 119 (1997) 62–69.

[5] J.Y. Jang, L.K. Chen, Numerical analysis of heat transfer and fluid flow in a three-dimensional wavy-fin and tube heat exchanger, Int. J. Heat Mass Transfer 40 (16) (1997) 3981–3990.

[6] C.A. McNab, K.N. Atkinson, M.R. Heikal, Numerical modeling of heat transfer and fluid flow over herringbone corrugated fins, Heat Transfer 1998 (6) (1998) 119–124.

[7] J. Min, R.L. Webb, Numerical predictions of wavy fin coil performance, J. Enhanced Heat Transfer 8 (2001) 159–173.

[8] L. Goldstein Jr., E.M. Sparrow, Experiments on the transfer characteristics of a corrugated fin and tube heat exchanger, ASME J. Heat Transfer 98 (1976) 26–34.

[9] L. Goldstein Jr., E.M. Sparrow, Heat/mass characteristics for flow in a corrugated wall channel, ASME J. Heat Transfer 99 (1977) 187–195.

[10] J.E. O'Brien, E.M. Sparrow, Corrugated-duct heat transfer, pressure drop, and flow visualization, ASME J. Heat Transfer 104 (1982) 410–416.

[11] M.M. Ali, S. Ramadyani, Experiments on convective heat transfer in corrugated channels, Exp. Heat Transfer 5 (1992) 175–193.

[12] D.R. Mirth, S. Ramadhyani, Correlations for predicting the air-side Nusselt numbers and friction factors in chilled-water cooling coils, Exp. Heat Transfer 7 (1994) 143–162.

[13] C.C. Wang, Y.J. Du, Y.J. Chang, W.H. Tao, Airside performances of herringbone fin-and-tube heat exchangers in wet conditions, Can. J. Chem. Eng. 77 (1999) 1225–1230.

[14] C.C. Wang, W.H. Tao, Y.J. Du, Effect of waffle height on the air-side performances of wavy fin-and-tube heat exchangers under dehumidifying conditions, Heat Transfer Eng. 21 (5) (2000) 17–26.

[15] ASHRAE Standard 33-78, Method of testing forced circulation air cooling and air heating coils, American Society of Heating, Refrigerating and Air-Conditioning Engineers, Inc, Atlanta, 1978.

[16] ASHRAE Standard 41.1-1986, Standard method for temperature measurement, american Society of Heating, Refrigerating and Air-Conditioning Engineers, Inc, Atlanta, 1986.

[17] ASHRAE Standard 41.2-1987, Standard methods for laboratory air-flow measurement, American Society of Heating, Refrigerating and Air-Conditioning Engineers, Inc, Atlanta, 1987.